Impact of single and double oxygen vacancies on electronic transport in Fe/MgO/Fe magnetic tunnel junctions

Beata Taudul, Martin Bowen, Mébarek Alouani

This is the accepted verion of an article that was published in Journal of Applied Physics. DOI: 10.1063/5.0019718

Impact of single and double oxygen vacancies on electronic transport in Fe/MgO/Fe magnetic tunnel junctions

Beata Taudul, M. Bowen, and M. Alouani

Université de Strasbourg, Institut de Physique et Chimie des Matériaux de Strasbourg, Unistra-CNRS UMR 7504, 23 Rue du Loess, BP 43, 67034 Strasbourg Cedex 2, France

(Dated: August 31, 2020)

Abstract

The combination of a low tunnelling barrier height and a large tunnelling magnetoresistance (TMR) ratio in MgO-class magnetic tunnel junctions (MTJs) has enabled next-generation information storage and bio-inspired computing solutions thanks to the spin transfer torque effect. Recent literature has proposed that this synergistic combination arises from the electronic properties of oxygen vacancies. To explicitly understand their impact on spin-polarized transport, we have computed the electronic and transport properties of single (F centers) and paired (M centers) oxygen vacancies using density functional theory and the projector augmented wave (PAW) method. These point defects can generate energy level positions of 0.4 eV with respect to the Fermi level for FeCo electrodes irrespective of the defect's spatial position within the MgO barrier, and of the orientation of the M center. These defects promote a strong decrease in the conductance of the spin up channel in the MTJ's parallel (P) magnetic state that mainly accounts for an order-of-magnitude drop in TMR, from ≈10000% in the ideal case toward values more in line with experiment. When placed in the middle layer of the MgO barrier, the F center introduces additional P ↑ transmission away from the Γ point. This scattering lowers TMR to 145%. In contrast, the M center merely broadens this transmission around Γ, thereby boosting TMR to 315%. Rotating a M center so as to partly point along the transmission direction sharpens transmission around Γ, further increasing TMR to 1423%. When these defects are placed at the MTJ interface, the transmission and ensuing TMR, which reaches ≈4000%, suggest that such junctions behave as would an ideal MTJ, only with a much lower TMR. Our results thus theoretically reconcile the concurrent observations of high TMR and low barrier heights, in line with experimental preparation techniques such as post-deposition oxidation of metallic Mg, which can generate oxygen vacancies at the lower MTJ interface, and annealing which can promote M centers over F centers. Our theory is also in line with an origin of perpendicular magnetic anisotropy in terms of oxygen vacancies at MTJ interfaces. The effective size of these vacancies sets a limit for both the barrier thickness, in line with experiment, as well as for the MTJ's lateral dimension. Our work provides a much-needed theoretical basis to move beyond the mostly unsuspected, fortuitous defect engineering of spintronic performance that has thus far propelled MgO-based spintronics and its applications.

PACS numbers: 71.15.Mb, 73.20.-r,73.40.-c,73.40.Qv

I. INTRODUCTION

Spintronic research exploits both charge and spin degrees of freedom in solid-state systems[1–4]. A widely studied spintronic device is the magnetic tunnel junction (MTJ), composed of two ferromagnetic metallic electrodes separated by an ultrathin dielectric. The electrical resistance of the MTJ depends on the relative orientation of the electrode magnetizations, which can be controlled by an external magnetic field or a spin-polarized current[5]. This change in resistance is called *tunnelling magnetoresistance* (TMR) and is defined as

$$TMR = \frac{R_{\mathrm{AP}} - R_{\mathrm{P}}}{R_{\mathrm{P}}}, \tag{1}$$

where R_{P} and R_{AP} are the resistances for parallel (P) and antiparallel (AP) configurations of the two magnetizations of the electrodes.

Initial MTJs with an Al_2O_3 tunnel barrier exhibited a maximum TMR of 70% at room temperature[6, 7]. Theoretical studies of magnetotransport across Fe/ZnSe/Fe[8] and Fe/MgO/Fe[8–12] MTJs revealed that the TMR can be greatly increased if the amorphous barrier is replaced by a crystalline one, such that certain orbitals with a high spin polarization in the electrodes preferentially tunnel across the barrier. Nowadays, textured FeCoB/MgO/FeCoB MTJs with TMR values above 600% at room temperature[13] offer promising prospects for data read-out, storage and processing, magnetic sensors[14–16].

Despite the importance of these MTJ technologies, an understanding of exactly how the device operates remains a work in progress. Indeed, the TMR effect is a complex phenomenon that depends strongly on the electronic structure of the electrodes, the properties of the insulating barrier and on the chemical bonding at the MTJ interface. As an illustration, consider how the success of achieving high TMR concurrently with low barrier heights required[17] to implement spin transfer torque toward these MTJ technologies[5, 14–16] imply that structural defects, which may lower TMR from the 10000% theoretical prediction, may actually play a beneficial spintronic role here.

Several causes for an effective deviation from the MTJ's ideal structure have been considered. Experiments often reveal the presence of interface oxidation, which alters the nature of chemical bonding at the interface between the ferromagnetic electrodes and the MgO spacer and can degrade TMR[18]. The combination of theoretical[19] and experimental[20] studies

showed that, even if one includes the interface disorder or the oxidation of interfacial Fe layer, the drastic drop of TMR cannot be fully explained by this mechanism alone.

As another cause, atomic diffusion may occur during the sample preparation and annealing[21]. In particular, boron diffusion into the MgO barrier (forming boron oxides), or its segregation at the CoFe/MgO interface, has been studied[22–25], but this is not always the case[26–28]. Rather, at a proper annealing temperature, boron does not diffuse into MgO but rather goes further away from the interfaces. Even if boron diffuses into MgO, it was shown theoretically that this should not create additional states within the MgO band gap[29].

Finally, another source can be imperfections in the MgO spacer itself, such as grain boundaries and point defects. The impact of the grain boundaries on the electronic structure and on the transport is difficult to address. Nonetheless, it was shown by Mizuguchi *et al.*[30] that the tunnelling current flows uniformly despite the existence of the grain boundaries and hence the device performance is not affected considerably by this kinds of defects. Moreover, the combined experimental and theoretical investigations of Bean *et al.*[31] showed that grain boundaries can cause a decrease of the effective barrier of MgO but this band gap decrease can not explain the observed low barrier heights[32].

Point defects, on the other hand, can promote localized states within the band gap of MgO, giving rise to a variety of interesting optical, catalytic and transport properties that are absent in the ideal crystalline material[33]. The most plausible imperfections are oxygen and magnesium vacancies, denoted F and V centers respectively. They can appear in a neutral, singly charged or doubly charged state that is denoted as F^{+}, F^{2+}, V^{-} V^{2-}, respectively. Moreover, two point defects can form a paired vacancy: two F centers form a F_2 pair of oxygen vacancies, which is a M center when they are nearest-neighbor on the oxygen sublattice. A F center can also combine with a V center to form a MgO vacancy.

As discussed by Gibson *et al.*[34], oxygen vacancies exhibit the lowest formation energy, which implies that this species of defects is more likely to occur in MgO. This defect species promotes localized states in the band gap of MgO and can affect the optical and the electrical properties of the dielectric[32, 34–36]. As a result, the barrier heights encountered by the propagating electrons are locally reduced[37, 38]. The electrons can then tunnel through the barrier using scattering states at the Fermi level, modified by the defect states, which are different from the scattering states for an ideal barrier as it can be seen later in Fig. 9.

This would explain experimental reports of a barrier height in MgO MTJs that is far below the nominal value of 3.9 eV (see Tab. I).

MTJ	TMR (%)	Barrier height (eV)
Fe/MgO/Fe	130 (190_{1K})	0.38/0.82[39]
Fe/MgO/Fe	180 (247_{20K})	0.39[40]
FeCo/MgO/FeCo	120-220	1.1-1.7[41]
FeCoB/MgO/FeCoB	100	0.62/0.5[32]
Fe/MgO/FeCo	$23_{4.2K}$/ 20_{70K}	0.9[42]

TABLE I. Experimental TMR and barrier heights for MTJs based on MgO.

Although oxygen vacancies within MgO appear to play an important role not only toward MTJ performance, but also spin transfer torque[17], their clear identification[43, 44] and impact on the tunnelling current has remained a work in progress. According to theory[35, 36, 45], single oxygen vacancies should create barrier heights of about 1.1 eV for the tunnelling electrons and decrease the resulting TMR. Even if we consider more F-type vacancies within MgO[45], the general conclusion is that these vacancies should degrade the TMR ratio[39]. On the other hand, in the presence of a 0.4 eV barrier height, coherent transport seem to be spintronically favorable[32, 40, 46]. Indeed, it was suggested by Schleicher *et al.*[32] that this barrier arise from M centers, which preserve coherent transport according to McKenna and Blumberg[46]. Only in a recent work, we have shown an unified experimental/theoretical picture of the potential landscape due to F and M centers[47, 48]. By studying the complex band structure of MgO with F and M centers we showed that the M centers reduce the barrier height in agreement with our experimental findings[47]. In a different study, we have shown that the energy positions of the F and M centers, with respect to the Fermi level, can be tuned by the choice of the type of the electrodes. In particular, this energy shift can be as large as 0.4 eV when the iron electrode is substituted by cobalt and was explained in terms of the change in the electrode work function [48].

In this work, we extend our previous studies[47, 48] by analyzing the electronic properties of F and M centers in MgO, and their impact on spin and symmetry polarized transport in Fe/MgO/Fe junctions employing density functional theory. The transport is calculated within the Landauer-Büttiker formalism as implemented in PWCOND[49]. We show that

the position of defect levels with respect to the Fermi level of the MTJs is robust against the type of exchange and correlation functional, and do not depend on the defect's spatial position in the barrier. Our results indicate that M centers can account for the experimental barrier height of 0.4 eV, and promote improved TMR relative to F centers. We also find that the defect's position within the barrier thickness strongly conditions spintronic performance. Relative to an ideal MTJ, this performance is mostly unaffected when the F or M center is close to an interface, but is reduced when the vacancy is moved onto the barrier's middle monolayer. In that case, rotating the M center restores stronger TMR. When judicious, we discuss how our theoretical framework of spintronic tunnelling across MgO in the presence of F and M centers adheres to experiment. The spatial extent of the F and M center suggest that a MTJ with a lateral size $\approx$ 2 nm can still exhibit high TMR[47].

The paper is organized as follows: In section II we present the details of our calculations and methodology. In sec. III we compute and discuss the electronic ground state properties of F and M centers either in bulk MgO or incorporated into MTJs. We compare the defect level positions obtained theoretically with the experimental data and discuss its change with respect to the types of electrodes. In sec. IV we show the results of transmission calculations for Fe/MgO/Fe MTJ with oxygen vacancies generated within MgO spacer. We explain the importance of the geometrical position of the vacancy with respect to the interface and the orientation of the defect plane for the M center. In the last section, we conclude the paper with a general discussion.

II. METHODOLOGY

A. Ground state calculations

To calculate the electronic structure of MgO with F and M centers, denoted as F(M)-MgO, we created the F/M centers by removing one/two neutral oxygen atoms from a simple cubic supercell containing 64 atoms. We used the experimental MgO lattice constant of $a_{\mathrm{MgO}} = 4.21$ Å. These calculations were performed using VASP package[50, 51] based on the projector augmented wave (PAW) method[52] and the Perdew, Burke, Enzerhof (PBE) generalized gradient approximation[53] for the exchange-correlation potential. The kinetic energy cutoff value of 500 eV for the plane wave basis set and the convergence criterion

for the total energy of 1μeV is used. The structures with defects were relaxed by requiring that the forces acting on atoms be less than 0.001 eV/Å. Due to the large size of the supercell, we found that a k-point mesh of 4×4×4 using the Methfessel-Paxton method with a smearing of $\tau = 0.2$ eV yields a satisfactory convergence of localized states resulting from these defects. Since it is well known that the generalized gradient approximation (GGA) underestimates the size of the band gap, we also used the hybrid Heyd, Scuseria, Ernzerhof (HSE) functional[54, 55] to correct the band gap and verify whether the defect level positions with respect to the Fermi level depends on the type of functional employed. The HSE hybrid functional mixes a portion of exact Fock exchange with that of DFT using an adjustable parameter μ. We found that, by increasing the Fock exchange to 43% in HSE06, we can reproduce the experimental band gap of MgO. This parameter is then used to calculate the defect levels in the MgO MTJs employing HSE06.

To determine the positions of the defect levels with respect to the Fermi energy and compare them with experiment, we used more realistic Fe/MgO/Fe MTJs. At the metal/insulator interface, the metallic electrode and the electronic transfer between the two materials and the metal induced gap states (MIGS) in the band gap of MgO will set the Fermi level position for the junction and establish the energy position of the defect levels accordingly. The geometry of the MgO/Fe supercell was based on the experimental results: the Fe conventional unit cell was rotated by a 45° with respect to that of MgO to match the lattice constants of both materials and avoid strains in the structure: $a_{\mathrm{MgO}} = \sqrt{2}a_{\mathrm{Fe}}$. In addition, oxygen atoms were placed on top of Fe atoms and the Fe-O distance at the interface was fixed to 2.17 Å following previous theoretical predictions[35, 56]. It is important to notice that the measured Fe-O distance is in the range of 2 Å[57, 58] to 2.2 Å[18]. We fixed the lattice constant of MgO to its experimental value ($a_{\mathrm{MgO}} = 4.21$ Å) and adjusted the lateral lattice parameter of the electrodes to it. This choice reflects the experimental evidence[59] that the annealing of FeCoB/MgO-based MTJs led to a recrystallization of the electrode/barrier interfaces so as to adopt the MgO lattice constant. The lattice parameter along the z axis was rescaled accordingly. The structure of the junction and relevant parameters are indicated in Fig. 1. Note because of the high CPU cost of HSE functional, the relaxation of the atoms around the F and M vacancies were conducted using only the PBE functional and no significant atomic motion was found in agreement with previous calculation of oxygen vacancies in MgO[68]. We have also found that the the lattice relaxation of the MgO supercell did not

change significantly the DOS with or without oxygen vacancies (not shown), however this lattice relaxation does not correspond to the real situation where the MgO slab is inserted between two semi-infinite metallic electrodes. Our calculation uses periodically repeated Fe/MgO/Fe slabs. To relax the geometry along the z direction one needs to study very large supercells as the inter-distance of many Fe and MgO layers near the interface will vary as it is shown in our previous study[60]. The full relaxation of the MTJs is CPU intensive a very cumbersome and will just complicate the study of the effect of F and M centers on the transport properties. As the aim of the present work is to compare the transport properties of F and M centers and show that the M centers are important for achieving higher TMR. We believe that this physics will not be significantly affected by the structural relaxation especially because it is found that the atomic relaxations around the F and M centers are negligible.

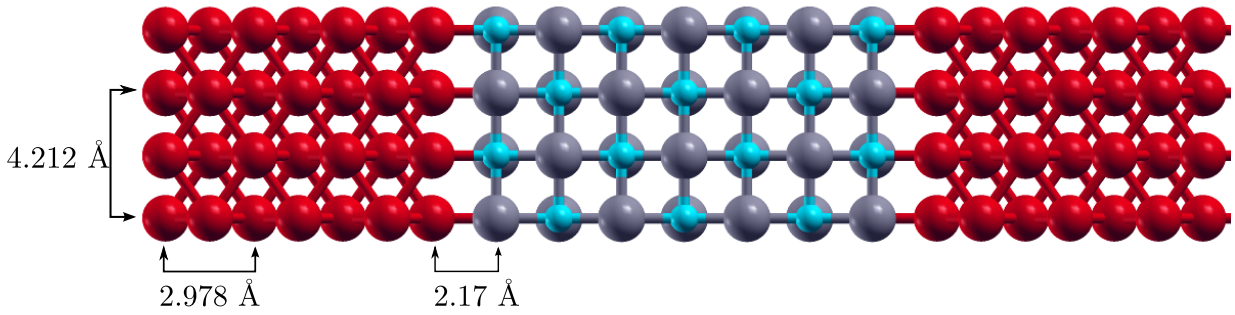

FIG. 1. Schematic representation of Fe/MgO junction with lattice parameters as indicated (Red atoms are Fe, blue O and grey Mg).

The experimental FeCoB electrodes are initially amorphous alloys whose interface with MgO adopts the latter's (001) texture upon annealing[59]. However, the exact arrangement of Fe and Co atoms is not really known. Moreover, the role of boron or its influence on the electronic structure of FeCo electrode is not clear. Therefore in our work we decided to consider a simplified scenario in which the FeCo electrode has the same structure as that of Fe. For the FeCo/MgO calculations, we have alternated the Fe and Co layers and chosen Co at the interface with MgO. Nonetheless, even the simplified structure can give us some insights into the impact of the type of electrode on the defect levels.

For the calculations involving full junctions, the kinetic energy cutoff value and the convergence criterion were the same as for the bulk MgO, but the value of τ was decreased to

0.1 eV and the spin polarized version of PBE-GGA was used. To compute the electronic structure of oxygen vacancies, the lateral directions of MTJ were doubled and periodic boundary conditions applied in all directions. The atoms around the oxygen vacancies were allowed to relax as described above.

B. Transport calculations

The ballistic conductance is calculated using Landauer-Büttiker[61, 62] formula

$$G(E_F) = \frac{e^2}{h} \sum_{n,\mathbf{k},\sigma} T_{n,\mathbf{k},\sigma}(E_F), \tag{2}$$

where $T_{n,k,\sigma}(E_F)$ is the total transmission at the Fermi energy and the summation is over all bands n crossing the E_F, for each $\mathbf{k}$ point and spin σ. Note that since the spin-orbit coupling is very small in the Fe/MgO/Fe MTJs and we are concerned only on the conductance at a very small bias, we ignored the spin mixing processes. The electron transmission was evaluated using the scattering based approach with a plane wave basis set and ultrasoft pseudopotential (USPP) scheme as implemented in the PWCOND[49] module of the Quantum Espresso (QE)[63] package. Note since the ballistic conductance is not yet implemented in VASP, we had to use QE to compute it. However, we had to make sure that both code generated the same electronic structure for MTJ electronic structure.

The conductance was evaluated between two semi-infinite electrodes connected by a scattering region that contains an insulating MgO spacer and a part of the leads on each side of the spacer. To compute the electron transmission at a given energy E, we first calculated the total energy of the ground state properties with the PWSCF code from QE package[63] and determined the effective potential. We then constructed the generalized Bloch states, including propagating and evanescent states, as a solution of Kohn-Sham equations at energy E for the infinite periodic leads, and the results were used to construct the scattering states and compute the transmission across the entire system. Moreover, in the spin density functional picture, electrons of different spin move independently in their different self-consistent potentials[49]. Therefore in this approach spin flip events are not included and the total transmission is the sum of the two spin channels such that $T(E) = T_{\uparrow}(E) + T_{\downarrow}(E)$.

To find how many electrode layers should be contained in the scattering region, we studied the changes of the electrostatic potential in the scattering region. To ensure that the

electron wave function changes smoothly at the interface between the bulk of the electrode and the scattering region, the part of the leads in the scattering region has to be big enough so that the changes induced in the electrostatic potential due to the interaction with MgO are contained entirely within the scattering region. If not, an artificial potential that scatters the incoming electrons could be present and might affect the results. By comparing the total electrostatic potential for the scattering region to the total potential of the bulk electrode, we found that from the 2nd-3rd monolayer (ML) of Fe, the bulk electrostatic potential is restored. In order to guarantee a proper geometrical matching between the scattering region and the electrodes, we used 4 ML of Fe on the left side of MgO and 5 ML of Fe on the right side. For the defect calculations, we doubled the lateral size of the junctions. When the antiparallel alignment of the electrodes was considered, the size of the junction along the z direction was doubled, such that the composition of the supercell was Fe(P)/MgO/Fe(AP)/MgO/F(P).

In the ground state calculations with PWSCF code, the cutoff energy values for the plane wave basis set and the electron density were set to 40 Ry and 400 Ry, respectively. The electronic occupations were broadened using a Gaussian smearing technique with a smearing parameter $\tau = 0.02$ Ry. The total energy convergence threshold was set to 10^{-8} Ry and the electron density mixing parameter to 0.1. Since we needed to use the same form of pseudopotential and the corresponding exchange-correlation functional for all atoms in the junction, we chose the Perdew and Wang (PW91) generalized gradient functional[64] in a spin-polarized form already generated and available in the QE library. For the ground state calculations of the ferromagnetic alignment of the electrodes, we used a **k**-point mesh of 5×5×1, while for the antiferromagnetic alignment the same **k**-point grid was slightly shifted out of the Γ point in order to speed up the convergence. Indeed to calculate the antiferromagnetic state we doubled the unit cell. This results in almost folded band structure producing numerically degenerate states along the high symmetry directions of the Brillouin zone. To avoid working with the eigenvectors of degenerate bands we shifted the **k**-point grid by half a step in each direction and required that the grid preserves the crystal symmetry.

An important factor in the transmission calculations is the convergence of the 2D basis set used in the PWCOND. Here, two parameters control the basis set: (i) *ewind* defines the energy window for reducing the 2D plane wave basis set in the transverse xy plane, and (ii) *epsproj* is a threshold for the 2D basis set reduction. The default values for the two

are *ewind* = 1 Ry and *epsproj* = 0.001, but in general, the larger the *ewind*, the smaller the *epsproj*, the higher the accuracy of the transmission. However, the increase in the transmission accuracy increases the computational cost and a suitable compromise should be found. These parameters were tested by examining the complex band structure (CBS) of bulk Fe and MgO[65, 66]. We found that *ewind* = 3, *epsroj* = 10^{-6} were sufficient to converge the CBS and hence they were used also to compute the transmission. In addition, the transmission was evaluated as a function of the number of **k** points in the 2D BZ. We tested meshes of 20×20, 30×30, 50×50 and 80×80 k-points and kept the 50×50 which showed a well-converged transmission.

III. ELECTRONIC STRUCTURE

A. MgO bulk

Here, we briefly describe the ground state electronic properties of M center within MgO bulk and MgO incorporated in the Fe(FeCo)/MgO MTJs. The removal of two neighboring oxygen atoms from an MgO supercell results in the creation of two occupied energy levels below E_{F}. The electrons that were transferred from Mg and remain after the oxygen removal are trapped and are mostly localized on the vacancy sites. Atomic relaxation showed that the atoms around the defect are only slightly distorted and the electronic structure of the defect is essentially not affected. This is due to the fact that the electron distribution on the vacancies resembles that of an oxygen O^{2-} ion. The distortions around the defect are therefore neglected[67]. In addition, the generation of double vacancy creates states near the minimum of conduction bands, which we refer as the excited states of M center (see Ref. [47] and Ref. [67] for details). These defect states could produce important features in optical spectra due to their localization within the defect region.

To understand the nature of the M center levels, we plot in Fig. 2 the orbital-projected band structure and the density of states (DOS) for MgO containing a M center (M-MgO). The valence states of MgO are mostly of O *p* character while the conduction states comprise Mg *s* and *p*-like states. The defect levels show mostly contributions form *p*-like orbitals with a smaller part coming from *s*-like states. By projecting the DOS on Mg and O sites (augmentation region of each site), we found that the M-levels are the results of a hybridization

between Op orbitals and both Mg s and p states. Note that the difference between the grey DOS and the red an green DOS comes from the interstitial region which is expended in plane waves. To get accurate symmetry one should use Wannier wave functions centered on the defect states. This quite involved calculation and is beyond the present study. The contribution of d-like states is much smaller and can be neglected. Note that the small dispersion around the Γ point is a result of an artificial interaction between the periodic images of the M centers due to the 64-atom size of our supercell. As we showed elsewhere[47], for supercells with 216 atoms, these levels exhibit no energy dispersion. This means that the defects are well separated from each other and spatially localized. Nonetheless, the dispersion observed for a 64-atom supercell does not significantly change the level positions, and as such it can be neglected.

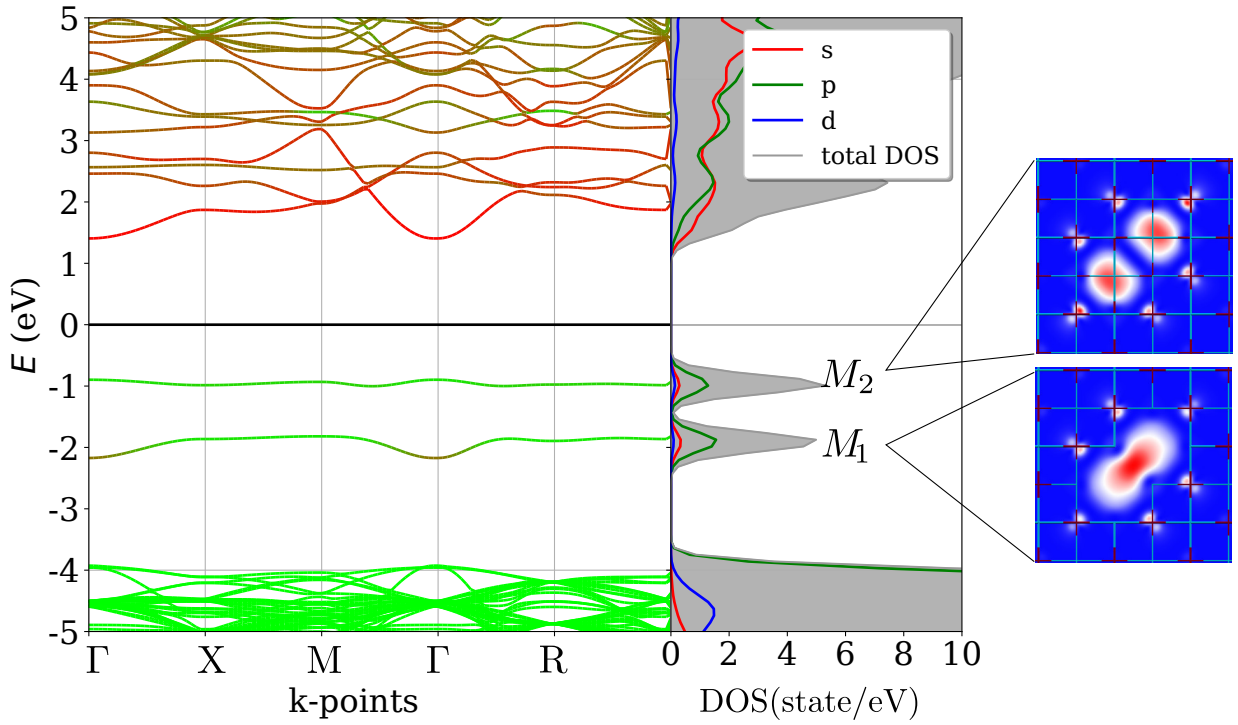

FIG. 2. Band structure and orbital projected DOS for M-MgO showing the symmetries of the bands. Insets show the electron distribution (linear scale) for each of the ground state energy levels of the M center. Red color indicates the region with the highest electron density 0.1 electron/Å^3 while blue denotes zero density.

We plot as insets to Fig. 2 the electronic spatial distribution for each of the M centers ground states. It is clear that the electron distribution for the M_1 state resembles a bonding-

like state, while it is anti-bonding for the M_2 state. As in the case of bond formation between atoms, the coupling between two F centers creates a bonding state with a lower energy, and an anti-bonding state with higher energy, with respect to the original F state energy level. Indeed, the F center peak is always positioned in between two M center ground states. As a consequence, the energy levels created by the F center is always higher than that associated with the M_1 state.

We emphasize that the nature of the MgO growth matters when comparing experiments with theoretical studies on nearly ideal MgO[68]. Annealing-induced control over the M/F ratio of centers is achieved only for dc-sputtered MgO, i.e., steps of Mg sputtering in Ar atmosphere plus oxidation to form the MgO; see Ref. [47] and not rf-sputtered MgO, i.e., one step of MgO sputtering in Ar atmosphere; see Ref. [69]. This is because dc-sputtered MgO has many more defects (including oxygen vacancies) than rf-sputtered MgO, in line with the resistance area (RA) products obtained (3 orders of magnitude lower for dc-MgO than rf-sputtered MgO). These experimental observations of a combined a) lack of control over the M/F ratio of centers and b) much higher RA products in rf-sputtered MgO MTJs are in line with the high diffusion barrier reported for the near pristine MgO in Ref. [68].

Figure 3 presents the spatial distribution of the electron density for both the ground (panels a/c) and excited (panels b/d) states of M-MgO. In panels a/b (c/d), a 214-atom (62-atom) supercell was used. We observe how neighboring oxygen vacancies hybridize to create an M center. As expected from the band structure plots, the electrons remaining after oxygen removal are localized on the vacancy sites and the electrons are distributed among the vacancies. Since the M center's excited state lies within the conduction band states, a nonzero electron density is present on atoms far from the defect. The electron density plots also reveal a hybridization between the M center states and the nearest oxygen ions, thereby showing that the defect level's excited state is indeed mostly of oxygen p character. The spatial electron density of the M center is fully isolated from the periodic images in the 214-atom supercell. Thus, the lateral extent of the M center spans 1 ML on either side of the oxygen vacancy sites that define the M center. On the other hand, spatial overlap develops between the electron density of M centers in the 62-atom supercell calculation. This means that M centers separated by 2 ML of MgO will experience electronic interactions. The electron distribution also indicates that the ground states of the M center are mostly s-like, while the excited states are of p-like character.

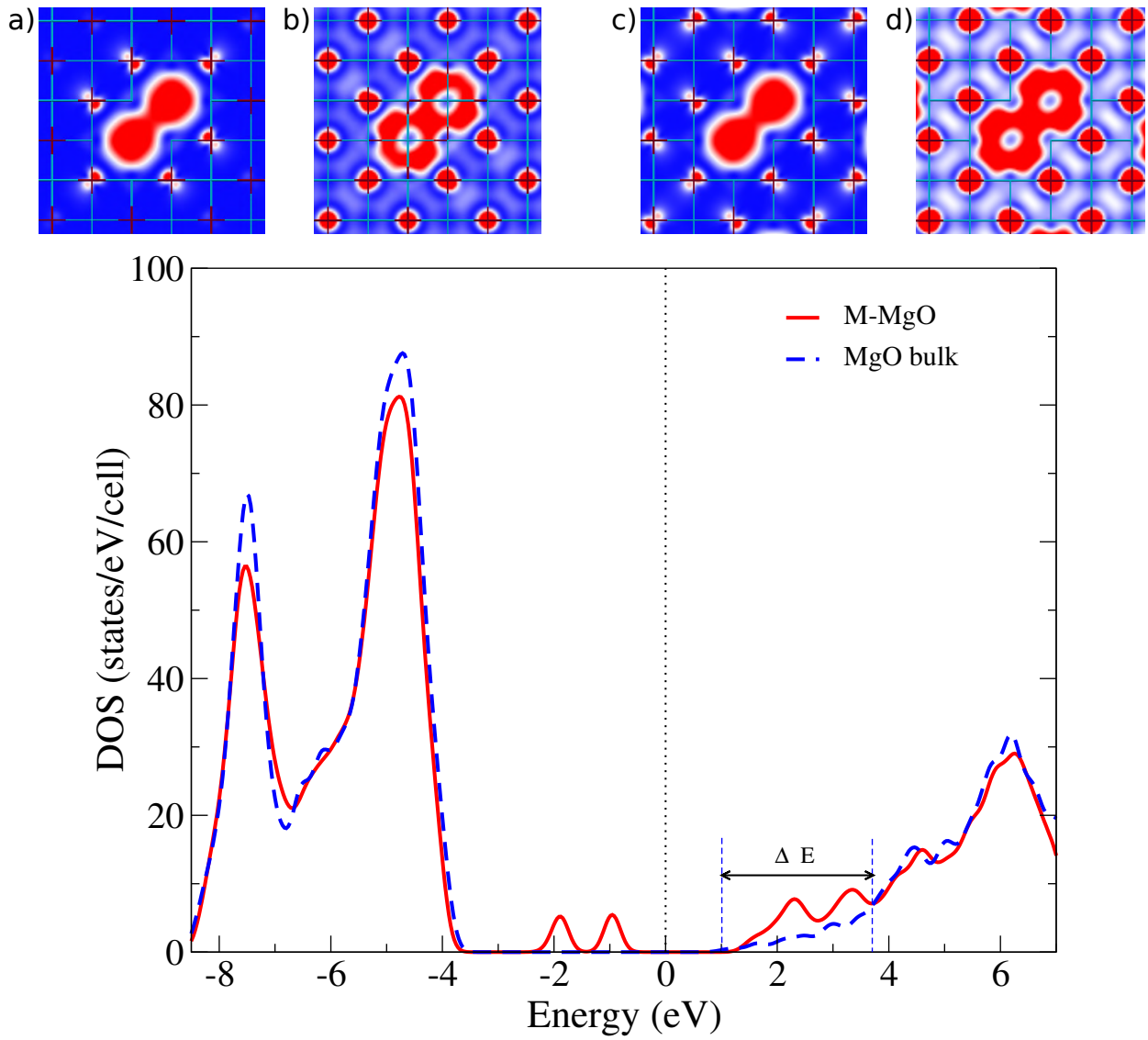

FIG. 3. Electron density distribution in the xy plane (linear scale), and within the energy range containing the M_1 and M_2 states (panels a/c) and M_1^* and M_2^* states (panels b/d), for a 214-atom supercell (panels a/b) and a 62-atom supercell (panels c/d).Red color indicates region with the highest electron density 0.1 electron/Å^3 while blue denotes zero density. The figure below shows the M-center MgO DOS compared to that of the bulk and shows the energy window (1 eV to 3.7 eV) used to determine the M_1^* and M_2^* electrons densities.

The results presented above are obtained within the GGA functional, which is known to underestimate the band gap. Therefore, as discussed in the methodology section, we also employed the HSE06 hybrid functional to accurately determine the defect level positions within the MgO band gap. Note that HSE06 was not used for computing the MTJ geometries

and transport because of the prohibitive CPU cost. Its use is only to justify whether or not the GGA Figure 4 presents the results of GGA and HSE06 bulk calculations for both M-MgO and MgO containing a F center (F-MgO), with E_{F} as calculated in self-consistent DFT procedure and set at the zero of energy in both calculations. For both F-MgO and M-MgO, compared to the GGA results, the hybrid functional causes a shifting of the valence and the conduction bands towards lower and higher energies, respectively. The hybrid functional, due to the inclusion of a portion of the exact Fock exchange which is orbital dependent, increases the localization by reducing the self-interaction error appearing in GGA. This fact has almost no influence on the F state position since it is a single localized level. However, in the case of a M center, where two additional energy levels are created in the MgO band gap, the difference can be noticeable and we observe a slight shift of the M_1 state further away from the M_2 level. This difference of the M_1 position between the GGA and the HSE06 calculations is about 0.27 eV. Nonetheless, aside from the shift in the M_1 energy position, we otherwise obtain a similar energy dependence of the DOS. We have checked that this type of comparison of HSE06 and GGA is appropriate by performing an HSE06 calculation of the DOS (not shown) of Fe/MgO(5ML)/Fe where the Fermi level is set by the Fe electrodes, and we observed the same energy shift of the top of valence state and bottom of conduction states of MgO, respectively, towards low and high energies. This shows how less intensive GGA-based calculations already yield a qualitatively correct picture of the electronic properties of oxygen vacancies in MgO. It is worth noticing that the defect levels are placed near the middle of the MgO band gap irrespective of the type of functional used. It clear that the HSE06 large band gap will make an overall renormalization of the conductance, but since the defect levels don't change with respect to the Fermi level, this common band gap reduction will not change the trend of the conductance for the various defects.

B. M-MgO/Fe(FeCo) junctions

We now calculate the electronic structure of both Fe/MgO/Fe and FeCo/MgO/FeCo junctions with oxygen vacancies in the MgO spacer layer. Fig. 5 presents the DOS projected on MgO(7ML) layers with F/M center generated in the middle 4th layer of the MgO spacer. Due to the contact with the metallic electrode, MIGS appear in the MgO band gap and

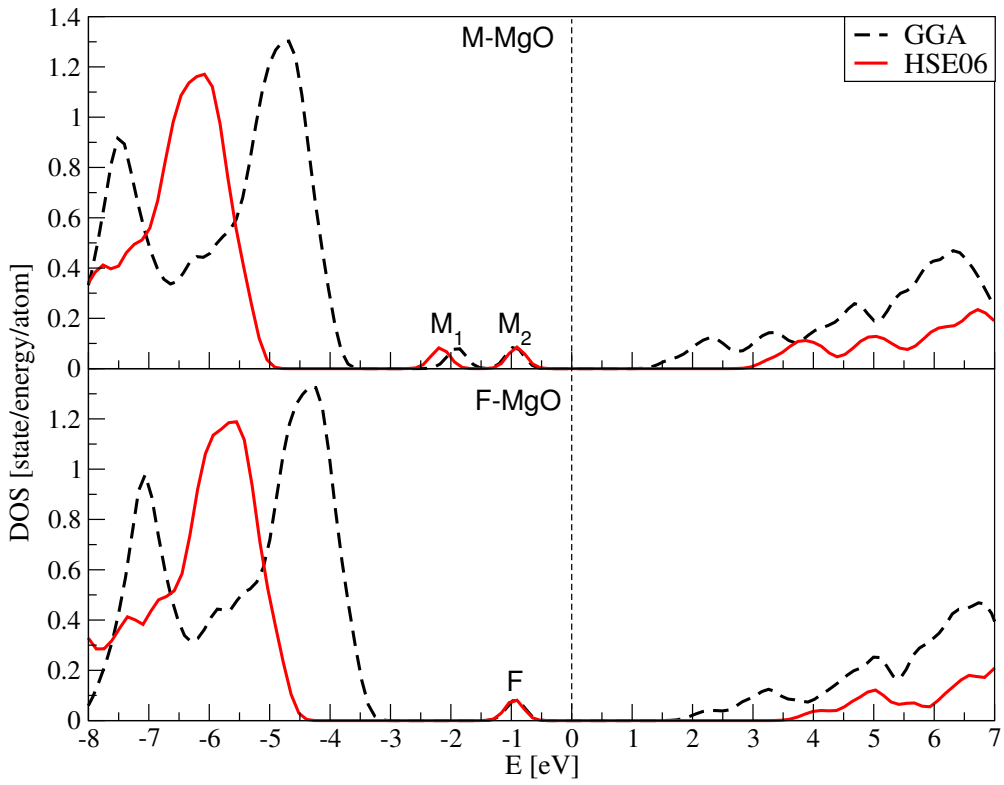

FIG. 4. GGA and HSE06 calculated DOS for bulk M-MgO (top panel) and F-MgO (bottom panel) with E_F aligned at the zero of energy for both functionals.

decay with the number of MgO layers. As a result the band gap of MgO disappears at the interface because of states coming from Fe. From the third layer the band gap of a bulk MgO is restored. Moreover, the ferromagnetic electrode induces spin polarization in the neighboring MgO layers and the difference in the DOS of spin up and down electrons can be clearly seen.

For the Fe/MgO heterostructures, the M_1 and M_2 states are located respectively at -1.7 eV and -0.7 eV below the Fermi level, while the F center level is at -1.2 eV. As expected the energy level associated with the F center is in between the M_2 and M_1 levels. In the case of the FeCo electrodes the defect levels are shifted towards the Fermi level by about 0.5 eV. It is worth noticing that not only are defect levels shifted, but also the whole band structure of MgO is rigidly shifted towards higher energies. This shift can be understood considering the 0.5 eV difference in the work function between Fe and Co. As before, the vacancy affects also the closest MgO layers up to 3 ML of MgO along the direction perpendicular to the M-center plane.

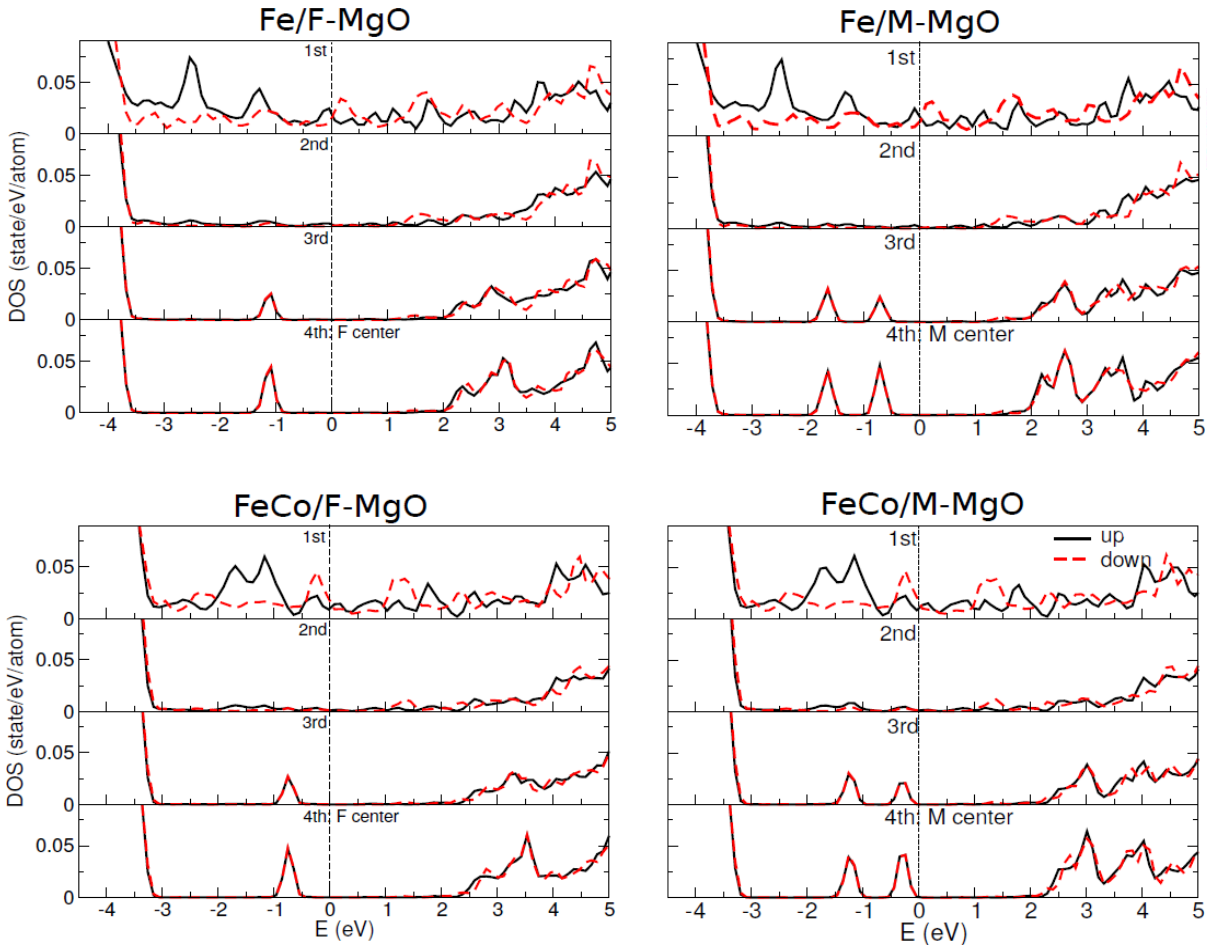

FIG. 5. Spin-polarized layer-projected DOS for Fe/F-MgO/Fe, Fe/M-MgO/Fe, FeCo/F-MgO/FeCo and FeCo/M-MgO/FeCo system with the F and M centers placed on the 4th layer.

We also studied the effect of shifting the M center within the MgO (7 ML) spacer and found that the defect energy level remains practically unchanged when the vacancy approaches the interface (data not shown)[67]. However, if the vacancy is placed on the interfacial MgO layer the DOS associated with the F/M center is washed out due to the strong interaction with the ferromagnetic electrode. Clearly, when the defect is closer to the interface, the hybridization between the two types of materials is strongly affected, which in turn influences the position of the Fermi level. However, it is surprising that this modification led only to a small differences in the Fermi level positions of the order of 0.09 eV.

Thus far, we have considered only the situation where the M center is in the plane parallel to the interfaces. In that case, we found that the effective size of the M center in the direction perpendicular to the interface reaches up to 3 ML of MgO due to charge transfer

onto adjacent MLs. We can also rotate the M center such that it can be partially aligned along the z direction and shared between two neighboring MgO layers. In that case, the effective M center size reaches 4 ML. Regardless of the orientation of the defect plane, the level position of the M center remains practically unchanged and similar results for the DOS are also obtained (not shown)[67]. Even though the changes in the DOS upon shifting or rotating the M center within the MgO spacer are not significant, we will show later that these changes have a huge impact on the transmission as hinted by complex band structure calculations[47]. Thus, based on our calculations, we can state that the computed energy range for energy levels associated with an M center can be associated with those measured experimentally at 0.4 eV, due to the M_2 state located $\approx$0.4 eV below the Fermi level for a FeCo/MgO/FeCo MTJ.

In the case of FeCo/MgO/FeCo MTJ, the interface termination will not affect the results substantially. What would change is the shape of DOS at the interfacial layer due to hybridization with Fe rather than Co. We have showed in Ref. [48] that the defect level positions can shift slightly for different electrodes; the cases of pure Fe and pure Co electrodes are the two extreme limits. In the case of CoFe/MgO termination, the defect levels should be slightly shifted towards lower energies with respect to FeCo/MgO termination. The transmission for the spin up channel in parallel electrode configuration for all types of electrodes, (Fe, Co and FeCo/Co) has in general the same shape and similar intensity, bigger differences are found in the spin down channel and AP configuration. The last two are affected by interfacial resonant states and are more sensitive to the changes at the interface.

In this study we did not consider a random distribution of oxygen vacancies because of the prohibitive computational cost for computing the transport properties of large supercells. Here our aim is to compare the F and M center as a function of its position in the barrier region. We considered how, by controlling the position of a precise oxygen vacancy species, one may alter magnetotransport. This reasoning is valid in the limit of a single nanoconduction channel that dominates transport, and in the limit of laterally nanoscaled junctions (down to 2 nm). It will be useful in future work to consider different vacancy configurations and concentration and their effect on TMR using a tight-binding model as performed Tsymbal *et al.*[70] and Klyukin *et al.*[71].

IV. BALLISTIC TRANSPORT

A. Ideal MgO-based junctions

We first calculated the transmission at the Fermi level for junctions with an ideal, 5 ML-thick MgO structure in order to examine the impact of introducing oxygen vacancies. The results found for the 7 ML spacer are similar to these for 5 ML and will be only briefly discussed.

Fig. 6 presents the transmission in the two dimensional Brillouin Zone (2D BZ) for the parallel electrode magnetization for the spin up and the spin down electron channels (left and middle panels) and the corresponding transmission for the antiparallel configuration (right panel). In agreement with previous theoretical predictions[56, 72], we found that the majority electron transmission is centered around the Γ point and dominated by the Δ_1 symmetry. The transmission for the minority channel occurs basically at the edges of the 2D BZ and is much smaller than for the majority channel. The transmission in the AP configuration is a mixture of features seen in both spin channels.

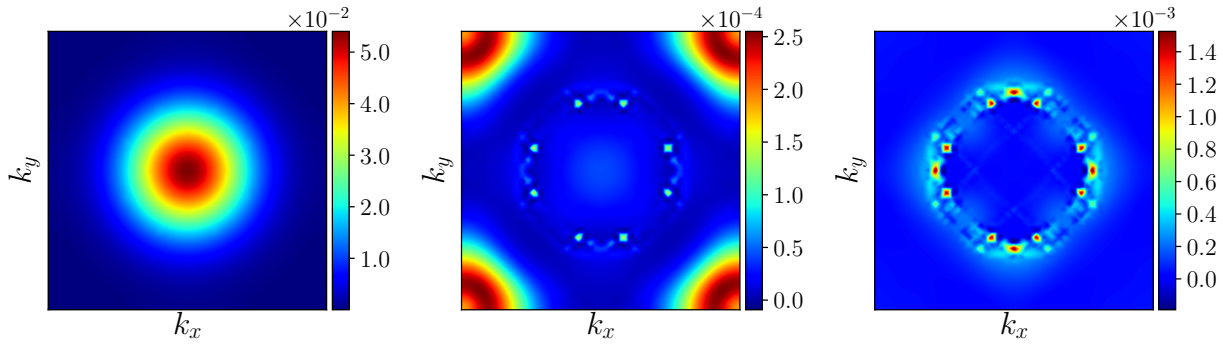

(a) (b) (c)

FIG. 6. Transmission in the two dimensional Brillouin zone (2D BZ) across an ideal Fe/MgO(5ML)/Fe junction in its P magnetic state for (a) the spin up channel, (b) the spin down channel, and (c) in its AP magnetic state.

By summing the transmission over the BZ for each channel, we obtain the conductance (see eq. 2) and the resulting TMR. Tab. II summarizes the transmission results for junctions with 5 and 7 ML of MgO. As expected, the transmission decays exponentially with the thickness of the MgO spacer and hence drops by at least one order of magnitude when

passing from 5 to 7 ML of MgO and the TMR increases with the number of MgO layers. This reflects the favorable symmetry filtering across MgO(001) of Δ_1 electrons with a high spin polarization at the bcc(001) Fe electrodes's Fermi level. For this reason, the Δ_1 channel is blocked in the MTJ's AP magnetic state, such that transmission is ensuring by Δ_5 and $\Delta_{2'}$ symmetry channels, which appear for both spin populations at E_F in Fe. When the MgO thickness is increased, the contributions to the conductance from the strongly attenuated Δ_5 and $\Delta_{2'}$ channels become smaller. This leads to a bigger overall difference in the transmission between the P and the AP configurations and causes the increase in TMR. According to literature[45], the TMR value should continue to grow at least up to 13 ML of MgO due to the dominant Δ_1 contribution.

B. F/M center in the middle layer of MgO

In the next step, we introduced single and double oxygen vacancies in the middle layer of the MgO spacer. Fig. 7(c) and 8(c) show the corresponding 2D BZ transmission for F and M centers, respectively. The BZ transmission distribution for P↓ is only slightly affected by the presence of the vacancies, resulting in a small increase in the total amplitude with respect to the ideal case (see Table II). However, in the spin up channel, a clear distinction in the P↑ transmission between the F and the M centers can be made. It appears that the F center scatters the propagating electrons to states with higher **k**-vectors. As a result, the transmission has a minimum at the Γ point and occurs mostly along k_x and k_y directions with maxima at the edges of the 2D BZ. The electrons are scattered symmetrically in each direction due to spherical symmetry of a single oxygen vacancy. On the other hand, the P↑ transmission in the presence of the M center becomes broadened in the 2D BZ but maintains a symmetric maximum at the vicinity of the Γ point. This clearly suggests that, while the transmission across a F center is reduced by an order of magnitude due to transport across k≠ 0 states, coherent transport that preserves spin and symmetry of the electron wave function is still possible when M center is present in the MgO spacer.

We found that, while F and M centers promote a reduction in total P↑ transmission (see Tab. II), both centers promote an increase in both the P↓ and AP total transmissions. Furthermore, the transmission distribution in the AP configuration changes significantly from that of an ideal MgO junction (see Fig. 6). While introducing defects reduces the

TMR, the TMR is higher for M centers compared to F centers. We found similar trends for the 7 ML , (see Tab. II). Again, if we increase the number of MgO layers (here from 5 to 7 ML), the TMR also increases regardless of the defect type.

In the theoretical model structures, the increase of MgO thickness results in a decrease of the defect concentration. The concentrations for F and M centers are respectively 2.5% and 5% for MTJs with 5 ML MgO and 1.78% and 3.57% for the 7 ML MgO. Nonetheless, as we have seen in the cases of 64 and 216 atom supercells with M(F) center concentration of 6.25%(3.13%) and 1.85%(0.93%) respectively, the reduced size of the supercell did not affect significantly the defect electronic properties. In the case of MTJs with increasing MgO thickness, the resulting TMR in presence of defects increases (Tab. II). This indicates the manifestation of symmetry filtering effects and the decreased impact of the defect states. However, the TMR for ideal MTJ is one order of magnitude larger than that of MTJ with oxygen vacancies and there is a clear distinction between F and M center even for smaller defect concentrations.

	P-UP	P-DOWN	AP	TMR [%]
Ideal 5ML	79.0	0.46	1.0	7850
F (5ML)	7.21	0.63	3.2	145
M (5ML)	17.1	1.47	4.5	315
Ideal 7ML	5.3	0.003	0.03	15770
F (7ML)	0.12	0.006	0.03	304
M (7ML)	0.62	0.007	0.04	1624

TABLE II. Total spin polarized transmissions $\times 10^4$ and TMR for Fe/MgO/Fe, Fe/F-MgO/Fe and Fe/M-MgO/Fe junctions, each with 5 and 7 ML of MgO. The F/M center is located in the middle layer.

Since the M center promotes higher TMR than the F centers in MgO MTJs with FeCo electrodes, these transmission results can account for the simultaneous experimental occurrence of high TMR alongside 0.4 eV barrier heights. They also confirm the initial assumption that coherent transport can be preserved when a M center is present.

Note that the defect level positions discussed previously were evaluated using the VASP code with the PAW basis set. To verify the robustness of these results, we switched to

a plane wave basis set in conjunction with an ultrasoft pseudopotential approach. While the shape of the layer-projected DOS is practically the same, we noticed a small shift of about 0.15 eV of the F and M_1 states towards lower energies. We then examined how this shift can influence the conductance by examining the transmission in the energy window $E_F \pm 0.1$ eV. In the case of the spin up transmission, the 2D BZ distribution and the amplitude of the transmission for all structures remains practically the same. However, some changes were observed in the spin down transmission. The likely cause is the presence of minority interfacial resonant states (IRS)[10]. This discrepancy should not influence the generality of the results presented since the contributions from the spin down channel to the G_{P} are much smaller than those of the spin up channel.

C. Effect of shifting the vacancy on the transmission

We now examine the impact of the position of the F and M centers within the barrier on spin-polarized transmission. Although we did not observe any significant change in the layer-projected DOS upon moving the vacancy to the interface, the transmission was nevertheless profoundly altered. Fig. 7(a) and 8(a) respectively show the 2D BZ spin-dependent transmissions with F and M centers generated in the interfacial MgO layer. Here, the M center always remains in the plane parallel to the interfaces. Interestingly, we found that the transmission distribution, for both defect types, is almost the same as for the ideal junction with the peaks amplitude very close to the ideal case (compare with Fig. 6). The calculated TMR reaches about 4261% and 3911% for the F and M center, respectively, i.e. are of the same order of magnitude as for the ideal junction (see Tab. III).

When vacancies are on the second layer from the interface, the transmission decreases and we observe additional sharp spikes in the P↑ channel (Figs. 7(b) and 8(b)). The P↓ and AP transmission distributions are only slightly affected. Note that the layer alternation also causes a rotation of the M center within the xy plane when we go from one layer to the next one. This explains the observed rotation in the transmission amplitude in the 2D BZ (compare for example panel (c) and (d) in Fig. 8).

To understand the changes in the transmission when varying the F/M centers position, we analyzed a real space distribution of scattering states at the Γ point. We discuss here the MTJ's P magnetic state, focusing on the spin up channel since its transmission strongly

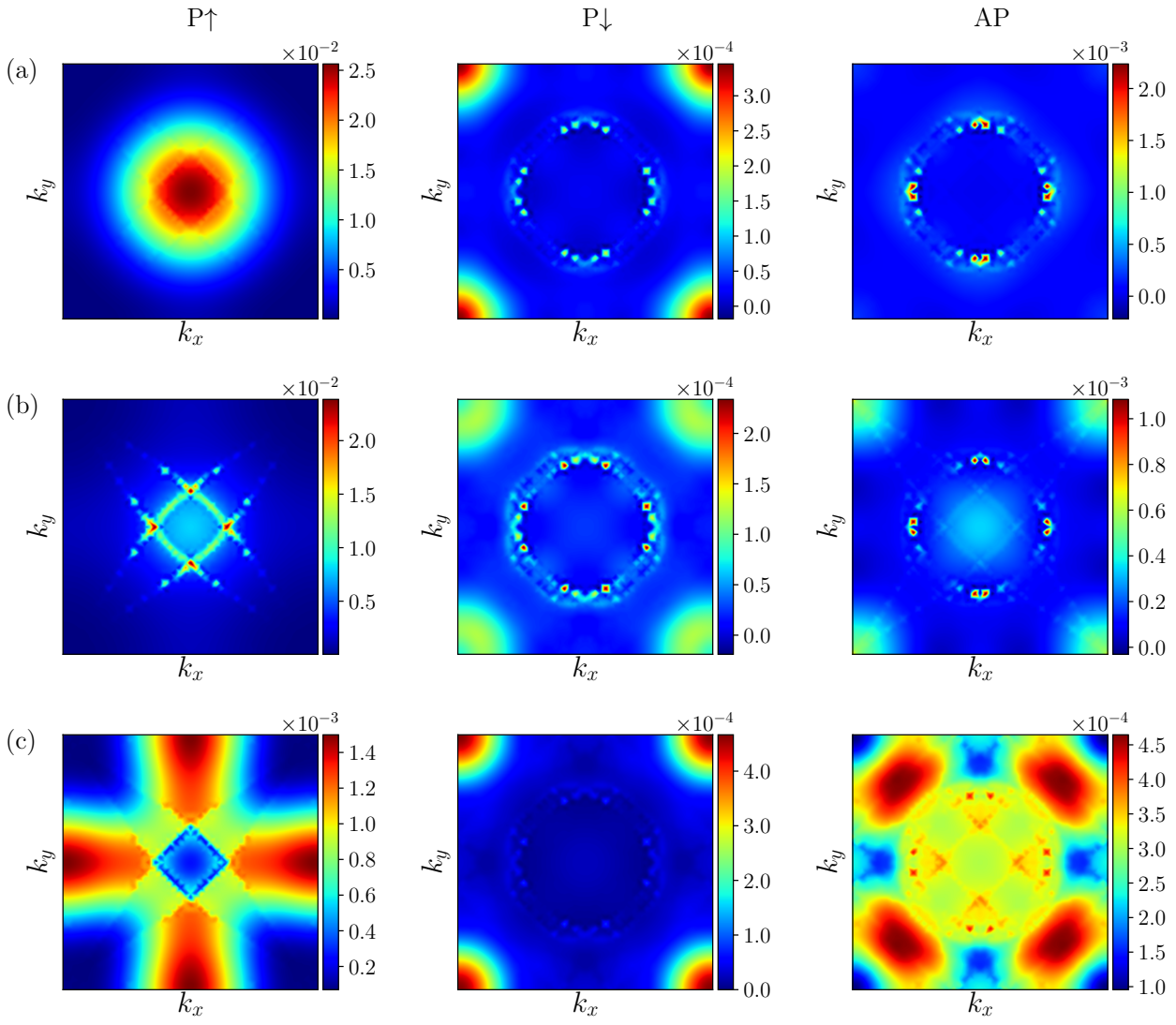

FIG. 7. Parallel alignment spin up (left) spin down (middle) and antiparallel (right) transmissions in the 2D BZ for Fe/F-MgO/Fe junction for 5 ML of MgO with F center in a) first ML (TMR=4261%), b) second ML (TMR=1239%) and c) third ML (TMR=145%).

drives the ensuing spintronic performance. In the spin up channel we focus on the Δ_1 symmetry since is has the smallest attenuation rate within MgO barrier and the biggest impact on the resulting transmission. Fig. 9 shows the density of a Δ_1 scattering state, summed over the xy plane, as a function of the position z along the transport direction for various defect configurations. Clearly, in the presence of vacancies, the amplitude of the Δ_1 channel is decreased with respect to the ideal case. Interestingly, M centers systematically yield a higher transmission amplitude than F centers at all defect positions within the barrier.

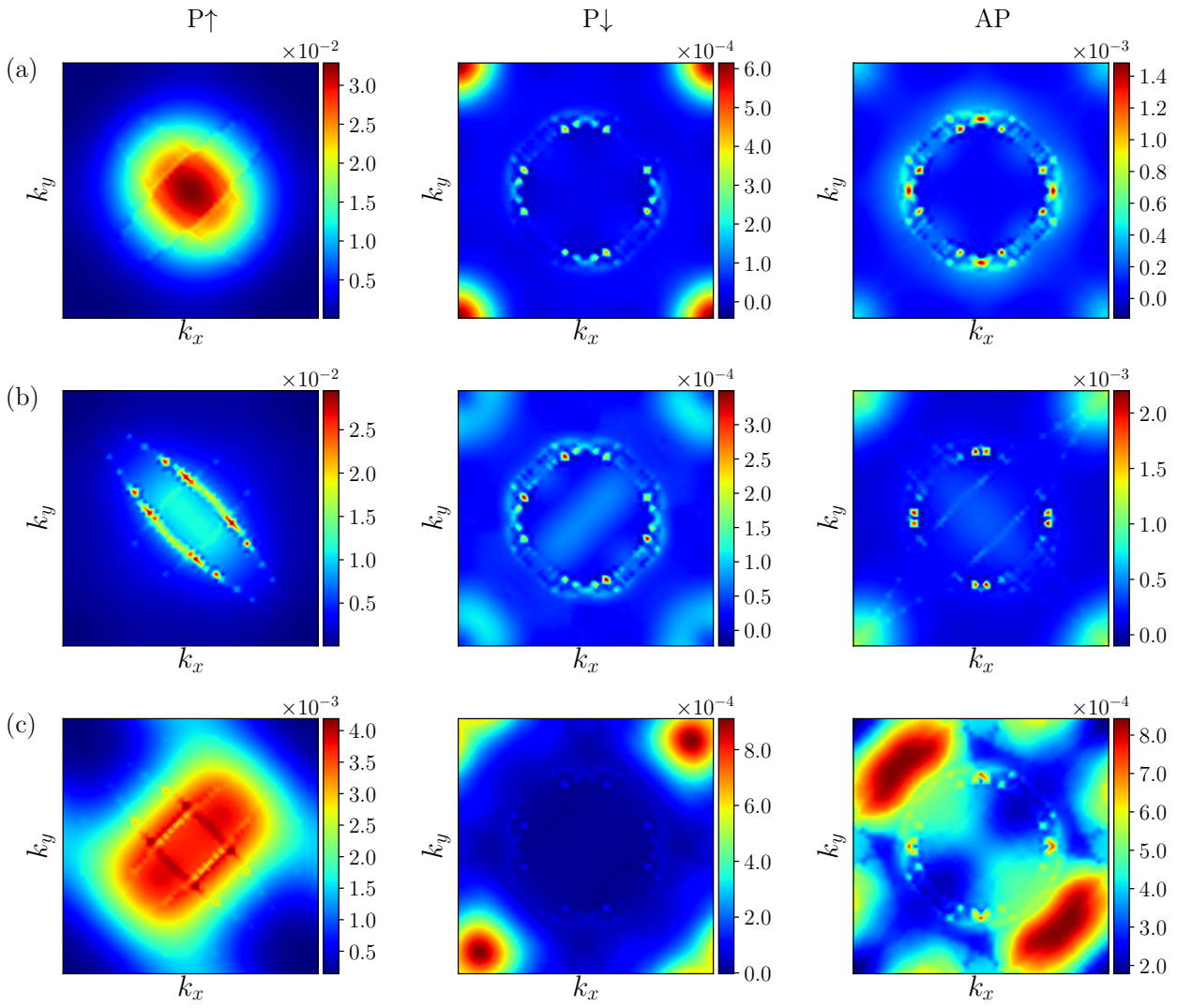

FIG. 8. Parallel alignment spin up (left) spin down (middle) and antiparallel (right) transmissions in the 2D BZ for Fe/M-MgO/Fe junction for 5 ML of MgO with M center in a) first ML (TMR=3911%), b) second ML (TMR=1135%) and c) third ML (TMR=315%).

Fig. 10 shows the Δ_1 scattering states at the Fermi level across a Fe/MgO(5ML)/Fe junction for the ideal case and the various positions of the F and M centers. All the data are normalized and the same logarithmic scale is used for comparison purposes.

As expected, in the case of an ideal junction, the Δ_1 channel originates from the left electrode, crosses the MgO barrier and ends in the right electrode. When F/M centers are introduced, the distribution of the Δ_1 state changes and depends on the vacancy type and position. The most beneficial configuration is with the vacancies located at the interfacial

TABLE III. Total spin polarized transmission$\times 10^4$ and TMR for Fe/F-MgO(5ML)/Fe and Fe/M-MgO(5ML)/Fe junctions with vacancies shifted within MgO layers.

	P-UP	P-DOWN	AP	TMR [%]
F in 1st ML	54.5	0.4	1.26	4261
F in 2nd ML	20.3	0.4	1.55	1239
F in 3nd ML	7.21	0.63	3.2	145
M in 1st ML	67.6	0.6	1.70	3911
M in 2nd ML	30.3	0.5	2.49	1135
M in 3nd ML	17.1	1.47	4.5	315

MgO layer. In that case, the amplitude of the scattering stated is just slightly lowered with respect to the ideal situation, and the Δ_1 channel is still transmitted from the left to the right electrode. Moreover, these graphs indicate that the further from the interface a vacancy is, the bigger the difference between F and M centers. The difference in distribution of the Δ_1 channel for F and M center in the third layer of MgO (Fig. 10) can explain the resulting values of TMR, 145% and 304% respectively, which underscores the synergistic spintronic role of M centers compared to F centers.

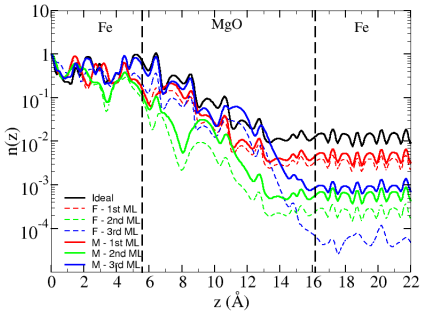

FIG. 9. Spin up Δ_1 scattering state distribution along the transport direction z for various vacancy configurations of Fe/F-MgO(5ML)/Fe and Fe/M-MgO(5ML)/Fe in the MTJ's P magnetic state. All the data are normalized and the same logarithmic scale is used.

The overall picture is that the transmission of the spintronically crucial Δ_1 spin up channel in the MTJ's P magnetic state in the presence of vacancies 1) is higher in presence of an M center rather than an F center for a defect positioned at the center of the barrier, and 2) is close to that of an ideal junction when either vacancy type is positioned near the interface.

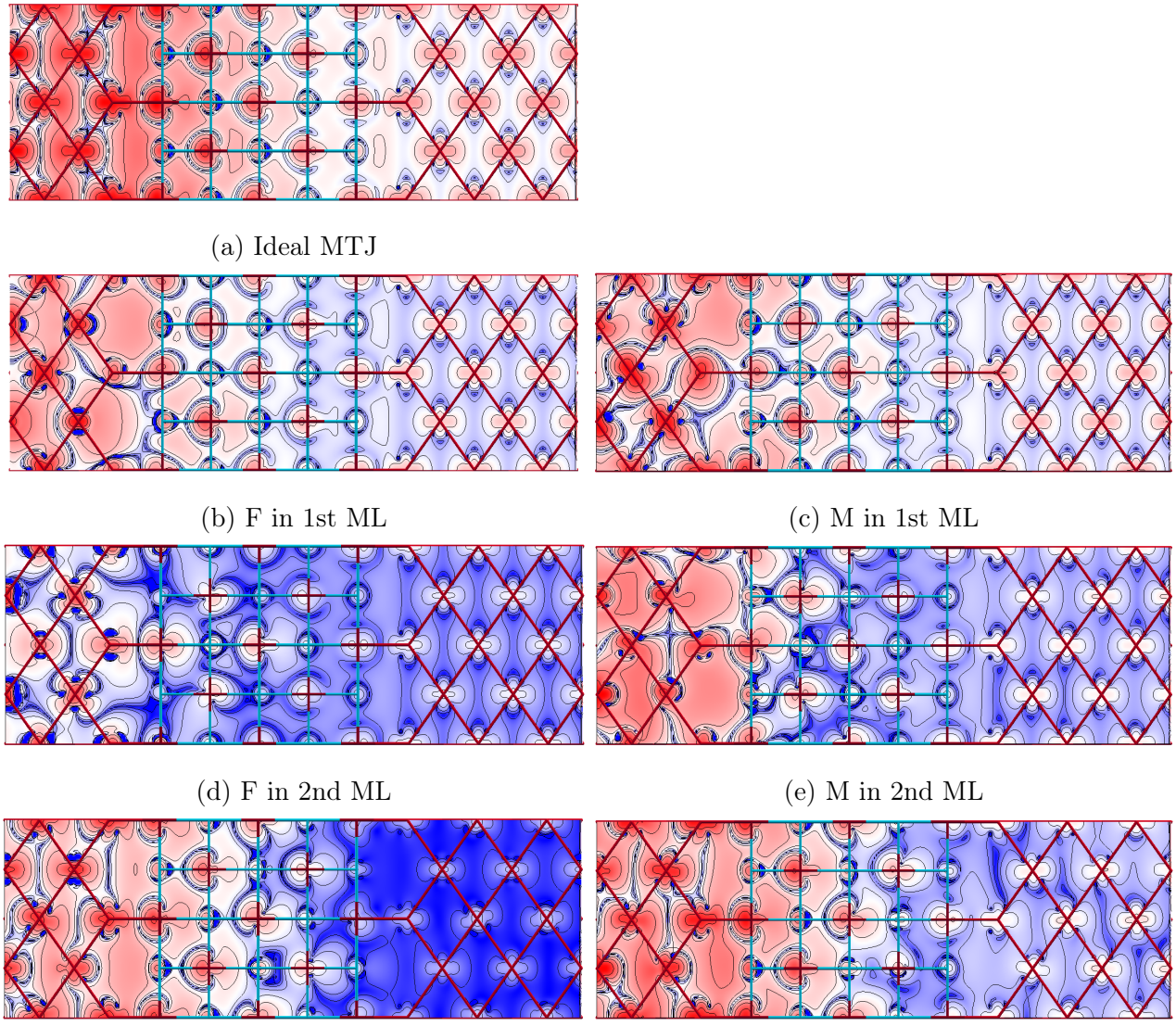

(a) Ideal MTJ

(b) F in 1st ML

(c) M in 1st ML

(d) F in 2nd ML

(e) M in 2nd ML

(f) F in 3rd ML

(g) M in 3rd ML

FIG. 10. 2D representation of the spin up Δ_1 scattering states in the x, z plane for various vacancy configurations of . All the data are normalized and the same logarithmic scale is used (see Fig. 9.

This second point sheds precious light into how a MgO-class MTJ can experimentally exhibit both high TMR and a low barrier height. Indeed, the MgO barrier is often formed atop the FeCoB metallic surface by sputtering metallic Mg, followed by an oxidation step[73, 74]. Avoiding the oxidation of the lower FeCoB interface can naturally lead to the presence of oxygen vacancies within the first ML of MgO. Interfacial oxygen vacancies also play a role in promoting perpendicular magnetic anisotropy for ultrathin ferromagnetic films in MTJs[75, 76]. Our results show that, counterintuitively, such states can maintain near-ideal levels of TMR and promote the low barrier height needed[17] for spin transfer torque.

Finally, our theoretical calculations indicate that a the formation energy of a M(F) center created at the interfacial MgO layer is lower by 2 eV (1 eV) than that of one one located on the center ML of a 5ML-thick MgO layer. This indicates that, indeed, interfacial defects are most probable to occur.

D. Rotating the M center

We now examine the impact on transmission of rotating the M center plane so that it is shared between two adjacent MgO layers. Prior complex band structure calculations[47] indicate that if the M center is located on two neighboring MgO layers parallel to the interface, the attenuation coefficient for the Δ_1 channel can be slightly smaller or comparable to the ideal case. To verify whether this attenuation is reflected in the transmission, we considered a symmetric junction with 6 ML of MgO, such that the M center is shared between the two middle layers. We also increased the number of electrode layers included in the scattering region to ensure proper geometrical matching at the interfaces.

Fig. 12 presents the transmission in the MTJ's P magnetic state for both spin channels, and in the AP magnetic state. Comparing with the ideal case (Fig. 6), we find that both the P$\downarrow$ and AP transmissions are practically unaffected by the defect. The spin up transmission is even more concentrated around the Γ point than before. The TMR value reaches 1423%, which is as high as when the F/M center is positioned next to the interfacial layer.

If we compare the spin up transmission in Fig. 12 and 8(c), we infer that the shape of the transmission reflects the symmetry/orientation of the M center. Indeed, when the M center is generated in a MgO plane parallel to the interfaces, the two oxygen vacancies lie along the diagonal, and a propagating electron simultaneously encounters both oxygen vacancies. This explains the elongation of the transmission peak along the diagonal of the plane in Fig. 8(c). On the other hand, when the M center is partially along the transport direction, i.e., in the yz plane, such that the two oxygen vacancies are in adjacent xy planes, the propagating electron reaches the first oxygen vacancy and then the second. As a result, the transmission is now along the k_y direction in the BZ (Fig. 12). The transmission peaks are of same intensity because, owing to the symmetrical MgO spacer, electrons propagating from the left and the right electrodes see the same potential landscape.

This preservation of high TMR thanks to a P$\uparrow$ transmission channel that is concentrated

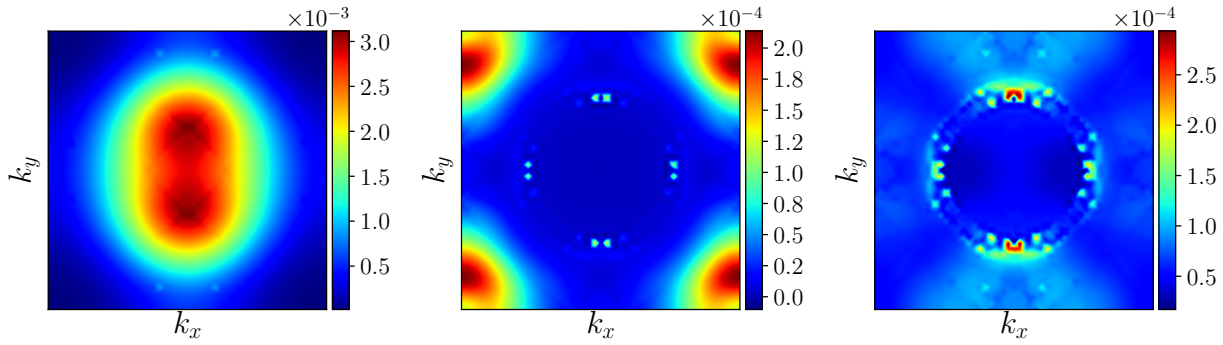

(a) (b) (c)

FIG. 11. Transmission in the two dimensional Brillouin zone (2D BZ) across an ideal Fe/MgO(5ML)/Fe junction in its P magnetic state for (a) the spin up channel, (b) the spin down channel, and (c) in its AP magnetic state.

FIG. 12. Transmission in the 2D BZ for Fe/M-MgO/Fe junction with 6 ML MgO spacer in its P magnetic state for (a) the spin up channel, (b) the spin down channel, and (c) in its AP magnetic state. Here the M center is located on the MgO 3rd and 4th ML in the yz plane.

at the Γ point illustrates how the scenario of a M center, at the barrier's center and partly directed along the tunnelling direction, can also concurrently generate high spintronic performance alongside a low barrier height.

V. CONCLUSION

We have analyzed the electronic properties of single (F centers) and paired (M centers) oxygen vacancies in bulk MgO and in the MgO spacer of Fe/MgO/Fe MTJs, and their impact on ballistic spin- and symmetry-polarized transport. As detailed below, we conclude that the experimental sample preparation techniques associated with the concurrent observation of high TMR and low barrier heights can be theoretically explained in terms of the presence of oxygen vacancies in the barrier, especially near a MTJ interface.

The M center generates two doubly occupied energy levels within the MgO band gap that mimic the bonding (M_1) and antibonding (M_2) atomic-like states created due to two interacting F centers. As a result, the M center's antibonding M_2 state generates a lower energy levels than does the F center. The energy level associated with a M_2 center is shifted

from -0.7 eV up to -0.2 eV below the Fermi level when we switch from an Fe to a Co interface, in agreement with the 0.5 eV change in work function of the Fe and Co surfaces. The M center's energy levels remain unchanged upon moving the M center from the MTJ interface to the barrier middle, and upon changing its orientation relative to the interfaces. Our results therefore explicitly ascribe the experimental barrier heights of 0.4 eV to the presence of paired oxygen vacancies within the MgO barrier.

Incorporating either a F or M center within a Fe/MgO/Fe magnetic tunnel junction can decrease the transmission of the P↑ channel, while increasing somewhat that of the P↓ and AP channels. As a result the theoretical TMR can drop by up to two orders of magnitude, from 10000% to 100%. Overall, M centers tend to maintain a transmission maximum at the Γ point for the P↑ channel, with only a small broadening, while F centers introduce scattering to higher **k**-vectors, thereby decreasing the channel's conductance. F and M centers induce only small increase in the P↓ and AP conductances. Consequently, the TMR is generally higher for transport across M centers than F centers. Since the calculated formation energy of an M center of 14.53 eV is lower than that of two F centers (14.65 eV) by 0.12 eV[67], annealing can induce the preferential presence of M centers over F centers, which in turn promotes higher spintronic performance[47]. This annealing-induced fusion of two F centers into a M center is possible only for a large nominal vacancy concentration as found in MgO grown by dc-sputtering Mg and post-deposition oxidation[47], rather than rf-sputtering MgO[69], in line with the high diffusion barrier for an oxygen vacancy in ideal MgO[68].

Our study indicates that the position of F and M centers crucially impacts magnetotransport. Compared to the case of an ideal junction, defects located on the interfacial MgO layer induce practically no change in either the shape of the transmission distribution or its amplitude. The resulting TMR reaches around 4000%, and the system amounts to an ideal MTJ with a barrier of reduced height and effective thickness. Moving the defect away from the interface reduces the P↑ transmission, and thus TMR, especially for the F center. This theoretical insight is compatible with the likely presence in experiments of oxygen vacancies at the lower MTJ interface when the MgO barrier is grown by oxidizing thin layers of metallic Mg deposited atop the lower ferromagnetic metallic electrode while avoiding the latter's oxidation[73, 74]. It is also in line with the role of interfacial oxygen vacancies in promoting perpendicular magnetic anisotropy in the adjacent ultrathin ferromagnetic films[75, 76] of

MgO-class MTJs with perpendicular magnetization. Finally, we find that orienting a M center at the barrier center so as to partly point along the transmission direction yields TMR 1000%.

Our study thus identifies conditions on the nature and positioning within the MgO of single/double oxygen vacancies so as to obtain predicted TMR values in excess of 1000% in MTJs with low barrier heights, in line with TMR amplitudes reported experimentally[13]. Our theoretical results thus reconcile the simultaneous presence of high TMR and low barrier heights in MgO-class MTJs by ascribing them to the presence of oxygen vacancies. Looking ahead, the respectively 3 ML and 3-4 ML effective physical size of the F and M centers condition not only the minimum barrier thickness for sizeable TMR (around 3 ML[77]), but also the MTJ's lateral size. Technological progress has enabled the demonstration of working MTJs with a lateral size down to 4.3 nm[78]. Experiments are thus approaching the 7-8 ML (i.e $\approx$2 nm) limit estimated for a M center to retain its electronic properties[47]. Our work provides a much-needed theoretical basis to move beyond the mostly unsuspected, fortuitous defect engineering of spintronic performance that has thus far propelled MgO-based spintronics and its applications.

ACKNOWLEDGMENTS

This work was performed using HPC resources from the Strasbourg Mesocenter and from the GENCI-CINES Grant gem1100. MB acknowledges funding from the Agence Nationale de la Recherche (ANR-14-CE26-0009-01) and the Labex NIE "Symmix" project (ANR-11-LABX-0058 NIE) and thanks F. Schleicher, D. Lacour, M. Hehn, F. Montaigne, S. Boukari and W. Weber for useful discussions.

DATA AVAILABILITY

The data that support the findings of this study are available from the corresponding author upon reasonable request.

---

[1] I. Žutić, J. Fabian, and S. Das Sarma, Rev. Mod. Phys. **76**, 323 (2004).

[2] A. Makarov, T. Windbacher, V. Sverdlov, and S. Selberherr, Semicond. Sci. Technol. **31**, 113006 (2016).

[3] J. W. Lu, E. Chen, M. Kabir, M. R. Stan, and S. A. Wolf, Int. Mater. Rev. **61**, 456 (2016).

[4] S. Z. Peng, Y. G. Zhang, M. X. Wang, Y. G. Zhang, and W. Zhao, in *Wiley Encyclopedia of Electrical and Electronics Engineering* (John Wiley & Sons, Inc., 2014), 12, pp. 1–16, ISBN 9780471346081.

[5] N. Locatelli, V. Cros, and J. Grollier, Nat. Mater. **13**, 11 (2013).

[6] J. S. Moodera, L. R. Kinder, T. M. Wong, and R. Meservey, Phys. Rev. Lett. **74**, 3273 (1995).

[7] D. Wang, C. Nordman, J. M. Daughton, Z. Qian, and J. Fink, IEEE Trans. Magn. **40**, 2269 (2004).

[8] J. M. MacLaren, X.-G. Zhang, W. H. Butler, and X. Wang, Phys. Rev. B **59**, 5470 (1999).

[9] W. H. Butler, X. G. Zhang, S. Vutukuri, M. Chshiev, and T. C. Schulthess, IEEE Trans. Magn. **41**, 2645 (2005).

[10] W. H. Butler, Sci. Technol. Adv. Mater. **9**, 014106 (2008).

[11] X.-G. Zhang and W. H. Butler, J. Phys. Condens. Matter **15**, R1603 (2003).

[12] W. H. Butler, X.-G. Zhang, T. C. Schulthess, and J. M. MacLaren, Phy. Rev. B **63**, 092402 (2001).

[13] S. Ikeda, J. Hayakawa, Y. Ashizawa, Y. M. Lee, K. Miura, H. Hasegawa, M. Tsunoda, F. Matsukura, and H. Ohno, Appl. Phys. Lett. **93**, 082508 (2008).

[14] A. D. Kent and D. C. Worledge, Nat. Nanotechnol. **10**, 187 (2015).

[15] C. Chappert, A. Fert, and F. N. V. Dau, Nat. Mater. **6**, 813 (2007).

[16] S. Ikeda, J. Hayakawa, Y. M. Lee, F. Matsukura, Y. Ohno, T. Hanyu, and H. Ohno, IEEE Trans. Electron Devices **54**, 991 (2007).

[17] U. Halisdemir, F. Schleicher, D. J. Kim, B. Taudul, D. Lacour, W. S. Choi, M. Gallart, S. Boukari, G. Schmerber, V. Davesne, et al., in *Society of Photo-Optical Instrumentation Engineers (SPIE) Conference Series* (2016), vol. 9931, p. 99310H.

[18] H. L. Meyerheim, R. Popescu, J. Kirschner, N. Jedrecy, M. Sauvage-Simkin, B. Heinrich, and R. Pinchaux, Phys. Rev. Lett. **87**, 076102 (2001).

[19] X.-G. Zhang, W. H. Butler, and A. Bandyopadhyay, Phys. Rev. B **68**, 092402 (2003).

[20] F. Bonell, S. Andrieu, A. M. Bataille, C. Tiusan, and G. Lengaigne, Phys. Rev. B **79**, 224405 (2009).

[21] J. Hayakawa, S. Ikeda, Y. M. Lee, F. Matsukura, and H. Ohno, Appl. Phys. Lett. **89**, 232510 (2006).

[22] T. Miyajima, T. Ibusuki, S. Umehara, M. Sato, S. Eguchi, M. Tsukada, and Y. Kataoka, Appl. Phys. Lett. **94**, 122501 (2009).

[23] X. Kozina, S. Ouardi, B. Balke, G. Stryganyuk, G. H. Fecher, C. Felser, S. Ikeda, H. Ohno, and E. Ikenaga, Appl. Phys. Lett. **96**, 072105 (2010).

[24] S. Pinitsoontorn, A. Cerezo, A. K. Petford-Long, D. Mauri, L. Folks, and M. J. Carey, Appl. Phys. Lett. **93**, 071901 (2008).

[25] A. K. Rumaiz, C. Jaye, J. C. Woicik, W. Wang, D. A. Fischer, J. Jordan-Sweet, and C. L. Chien, Appl. Phys. Lett. **99**, 222502 (2011).

[26] H. Kurt, K. Rode, K. Oguz, M. Boese, C. C. Faulkner, and J. M. D. Coey, Appl. Phys. Lett. **96**, 262501 (2010).

[27] S. Mukherjee, R. Knut, S. M. Mohseni, T. N. Anh Nguyen, S. Chung, Q. Tuan Le, J. Åkerman, J. Persson, A. Sahoo, A. Hazarika, et al., Phys. Rev. B **91**, 085311 (2015).

[28] Z. Wang, M. Saito, K. P. McKenna, S. Fukami, H. Sato, S. Ikeda, H. Ohno, and Y. Ikuhara, Nano Lett. **16**, 1530 (2016).

[29] Z. Bai, L. Shen, Q. Wu, M. Zeng, J.-S. Wang, G. Han, and Y. P. Feng, Phys. Rev. B **87**, 014114 (2013).

[30] M. Mizuguchi, Y. Suzuki, T. Nagahama, and S. Yuasa, Appl. Phys. Lett. **91**, 012507 (2007).

[31] J. J. Bean, M. Saito, S. Fukami, H. Sato, S. Ikeda, H. Ohno, Y. Ikuhara, and K. P. McKenna, Sci. Rep. **7**, 45594 (2017).

[32] F. Schleicher, U. Halisdemir, D. Lacour, M. Gallart, S. Boukari, G. Schmerber, V. Davesne, P. Panissod, D. Halley, H. Majjad, et al., Nat. Commun. **5**, 4547 (2014).

[33] G. H. Rosenblatt, M. W. Rowe, G. P. Williams, R. T. Williams, and Y. Chen, Phys. Rev. B **39**, 10309 (1989).

[34] A. Gibson, R. Haydo, and J. P. LaFemina, Phy. Rev. B **50**, 2582 (1994).

[35] J. P. Velev, K. D. Belashchenko, S. S. Jaswal, and E. Y. Tsymbal, Appl. Phys. Lett. **90**, 072502 (2007).

[36] J. P. Velve, M. Y. Zhuravlev, K. D. Belashchenko, S. S. Jaswal, E. Y. Tsymbal, T. Katayama, and S. Yuasa, IEEE Trans. Magn. **43**, 2770 (2007).

[37] D. J. Kim, W. S. Choi, F. Schleicher, R. H. Shin, S. Boukari, V. Davesne, C. Kieber, J. Arabski,

G. Schmerber, E. Beaurepaire, et al., Appl. Phys. Lett. **97**, 263502 (2010).

[38] M. Studniarek, U. Halisdemir, F. Schleicher, B. Taudul, E. Urbain, S. Boukari, M. Hervé, C.-H. Lambert, A. Hamadeh, S. Petit-Watelot, et al., Adv. Mater. **29** (2017), 1606578.

[39] G. Miao, Y. Park, J. Moodera, M. Seibt, G. Eilers, and M. Münzenberg, Phys. Rev. Lett. **100**, 246803 (2008).

[40] S. Yuasa, T. Nagahama, A. Fukushima, Y. Suzuki, and K. Ando, Nat. Mater. **3**, 868 (2004).

[41] S. S. P. Parkin, C. Kaiser, A. Panchula, P. M. Rice, B. Hughes, M. Samant, and S.-H. Yang, Nat. Mater. pp. 862–867 (2004).

[42] S. Mitani, T. Moriyama, and K. Takanashi, J. Appl. Phys. **93**, 8041 (2003).

[43] Y. Lu, M. Tran, H. Jaffrès, P. Seneor, C. Deranlot, F. Petroff, J. M. George, B. Lépine, S. Ababou, and G. Jézéquel, Phys. Rev. Lett. **102**, 176801 (2009).

[44] J. M. Teixeira, J. Ventura, J. P. Araujo, J. B. Sousa, P. Wisniowski, S. Cardoso, and P. P. Freitas, Phys. Rev. Lett. **106**, 196601 (2011).

[45] Y. Ke, K. Xia, and H. Guo, Phys. Rev. Lett. **105** (2010).

[46] K. P. McKenna and J. Blumberger, Phys. Rev. B **86**, 245110 (2012).

[47] B. Taudul, E. N. Monteblanco, U. Halisdemir, D. Lacour, F. Schleicher, F. Montaigne, E. Beaurepaire, S. Boukari, M. Hehn, M. Alouani, et al., Adv. Electron. Mater. **3**, 1600390 (2017).

[48] F. Schleicher, B. Taudul, U. Halisdemir, K. Katcko, E. Monteblanco, D. Lacour, S. Boukari, F. Montaigne, E. Urbain, L. M. Kandpal, et al., J. Phys. D **52**, 305302 (2019).

[49] A. Smogunov, A. D. Corso, and E. Tosatti, Phys. Rev. B **70**, 045417 (2004).

[50] G. Kresse and J. Furthmüller, Phys. Rev. B **54**, 11169 (1996).

[51] G. Kresse and D. Joubert, Phys. Rev. B **59**, 1758 (1999).

[52] P. E. Blöchl, Phys. Rev. B **50**, 17953 (1994).

[53] J. P. Perdew, K. Burke, and M. Ernzerhof, Phys. Rev. Lett. **77**, 3865 (1996).

[54] J. Paier, M. Marsman, K. Hummer, G. Kresse, I. C. Gerber, and J. G. Ángyán, J. Chem. Phys. **124**, 154709 (2006).

[55] F. Viñes, O. Lamiel-García, K. Chul Ko, J. Yong Lee, and F. Illas, J. Comput. Chem. **38**, 781 (2017).

[56] W. H. Butler, X.-G. Zhang, T. C. Schulthess, and J. M. MacLaren, Phys. Rev. B **63**, 054416 (2001).

[57] T. Urano and T. Kanaji, J. Phys. Soc. Jpn. **57**, 3403 (1988).

[58] W. Wulfhekel, M. Klaua, D. Ullmann, F. Zavaliche, J. Kirschner, R. Urban, T. Monchesky, and B. Heinrich, Appl. Phys. Lett. **78**, 509 (2001).

[59] J. Hayakawa, S. Ikeda, F. Matsukura, H. Takahashi, and H. Ohno, Jpn. J. Appl. Phys. **44**, L587 (2005).

[60] X. Feng, O. Bengone, M. Alouani, S. Lebègue, I. Rungger, and S. Sanvito, Phys. Rev. B **79**, 174414 (2009).

[61] R. Landauer, Zeitschrift für Physik B Condensed Matter **68**, 217 (1987).

[62] M. Büttiker, Y. Imry, R. Landauer, and S. Pinhas, Phys. Rev. B **31**, 6207 (1985).

[63] P. Giannozzi, S. Baroni, N. Bonini, M. Calandra, R. Car, C. Cavazzoni, D. Ceresoli, G. L. Chiarotti, M. Cococcioni, I. Dabo, et al., J. Phys. Condens. Matter **21**, 395502 (2009).

[64] J. P. Perdew and Y. Wang, Phys. Rev. B **45**, 13244 (1992).

[65] J. P. Velev, K. D. Belashchenko, D. A. Stewart, M. van Schilfgaarde, S. S. Jaswal, and E. Y. Tsymbal, Phys. Rev. Lett. **95**, 216601 (2005).

[66] M. Bowen, A. Barthélémy, V. Bellini, M. Bibes, P. Seneor, E. Jacquet, J. P. Contour, and P. Dederichs, Phys. Rev. B **73**, 140408 (2006).

[67] B. Taudul, Ph.D. thesis, Université de Strasbourg, Institut de Physique et Chimie des Matériaux de Strasbourg (2017), thèse de doctorat dirigée par Alouani, Mébarek Physique Strasbourg 2017, URL `http://www.theses.fr/2017STRAE042/document`.

[68] J. Carrasco, N. Lopez, and F. Illas, Phys. Rev. Lett. **93**, 225502 (2004).

[69] F. Schleicher, U. Halisdemir, E. Urbain, D. Lacour, M. Gallart, S. Boukari, F. Montaigne, E. Beaurepaire, P. Gilliot, M. Hehn, et al., J. Phys. D **48**, 435004 (2015).

[70] E. Y. Tsymbal, A. Sokolov, I. F. Sabirianov, and B. Doudin, Phys. Rev. Lett. **90**, 186602 (2003).

[71] K. Klyukin, L. L. Tao, E. Y. Tsymbal, and V. Alexandrov, Phys. Rev. Lett. **121**, 056601 (2018).

[72] J. Mathon and A. Umerski, Physical Review B **63**, 220403(R) (2001).

[73] F. Dahmani, Jpn. J. Appl. Phys. **73**, 043002 (2012).

[74] R. W. Dave, G. Steiner, J. M. Slaughter, J. J. Sun, B. Craigo, S. Pietambaram, K. Smith, G. Grynkewich, M. DeHerrera, J. Åkerman, et al., IEEE Trans. Magn. **42**, 1935 (2006).

[75] H. X. Yang, M. Chshiev, B. Dieny, J. H. Lee, A. Manchon, and K. H. Shin, Phys. Rev. B **84**, 054401 (2011).

[76] B. Dieny and M. Chshiev, Rev. Mod. Phys. **89**, 025008 (2017).

[77] W. Skowronski, T. Stobiecki, J. Wrona, K. Rott, A. Thomas, G. Reiss, and S. van Dijken, J. Appl. Phys. **107**, 093917 (2010).

[78] K. Watanabe, B. Jinnai, S. Fukami, H. Sato, and H. Ohno, Nat. Commun. **9**, 663 (2018).